Hindawi
International Transactions on Electrical Energy Systems
Volume 2023, Article ID 1869840, 15 pages
https://doi.org/10.1155/2023/1869840

Research Article

Design and Robustness Analysis of Multiple Extended State Observer Based Controller (MESOBC) for AVR of the Power System

Ravi Gandhi,[1] S. B. Masikana,[2] Gulshan Sharma ,[3] and Emre Çelik [4]

[1]*School of Engineering, Ajeenkya DY Patil University, Pune 412105, India*
[2]*Department of Electrical Engineering, Mangosuthu University of Technology, Durban & Department of Electrical Engineering Technology, University of Johannesburg, Johannesburg 2006, South Africa*
[3]*Department of Electrical Engineering Technology, University of Johannesburg, Johannesburg 2006, South Africa*
[4]*Department of Electrical and Electronics Engineering, Engineering Faculty, Düzce University, Düzce, Turkey*

Correspondence should be addressed to Gulshan Sharma; gulshanmail2005@gmail.com

Received 25 September 2022; Revised 30 October 2022; Accepted 1 March 2023; Published 10 March 2023

Academic Editor: Ramesh Chand Bansal

Automatic voltage regulator (AVR) is installed on the synchronous generators in the power system and plays a very important role in maintaining the generator output voltage besides changes in load demand, parametric uncertainties, and operating temperature. As the load is continuously varying in the system, the AVR needs controllers to track and regulate the voltage of the synchronous generator much faster. This paper shows an initial attempt to design a robust multiple extended state observer (MESO) to estimate the variation in lump disturbances (i.e., load demand and parametric uncertainties) from all the components of the AVR. MESO-based controller (MESOBC) can track such matching and mismatching of both types of irregularities and regulate the terminal voltage of the generator accordingly. MESOBC performance is matched with strong published AVR designs for a standard condition, ±30% load voltage variation and for simultaneous changes in AVR parameters with ±30% load voltage variations. Integrated square error (ISE) is chosen as an objective function to compare the output of MESOBC with other published AVR designs in view of graphical AVR responses and by calculating various numerical values for AVR responses. At last, the robustness of MESOBC is also checked through sensitivity analysis, and it is seen that MESOBC guaranteed robust performance for the AVR of the power system under diverse operating conditions.

1. Introduction

The modern power system is complex and getting wider and wider these days to meet the continuous electrical energy demands of the society and nation. Any successful power system needs to maintain the voltage and frequency of the power system very tightly to its nominal value. However, due to the shifting of consumers' electrical energy demands, it is very difficult to maintain these electrical parameters, and ultimately it results in the insufficiency of the power system to deliver quality electrical energy to various customers. The AVR is a feedback control system which measures the current synchronous generator output voltage and matched it with the reference voltage value, and hence an error signal is generated. This error signal is used to manage the excitation of the synchronous generator, and thus the AVR can increase or decrease the generator output voltage considering that voltage should be within its tight band as per the system requirements. However, synchronous generator output voltage shows a very slow response due to varying load and high alternator field windingsinductance [1]. Hence, a controller is a must for the AVR of the power system to achieve a faster response with minimum overshoot, reduced settling time, and zero steady-state error for various disturbances. Various types of controllers such as PID, PID with acceleration (PID-A), fractional order developed PID, and controllers built on various concepts of fuzzy logic are available for the AVR in [2–6]. Recently,

researchers have used optimization techniques to tune the values of controllers due to variable operating conditions, high order, and due to nonlinear load patterns of the power system. Genetic algorithm (GA) was the simplest and first optimization technique explored for power system application [7]. After GA, number of optimization techniques such as bat search, harmony search technique, gravitational search algorithm [8–11], and most recently teaching learning-based optimization (TLBO) algorithms [12, 13] emerge as powerful optimization for various applications of the power system. In [14], authors have shown that the design of PID built on PSO outperforms GA for the AVR. In [15], authors have concluded that the ant colony optimized design of PID is much better than PSO and GA. The authors have successfully shown that the artificial bee colony (ABC) algorithm is capable to provide the optimal response for the AVR, and the performance of ABC is matched with particle swarm optimization (PSO) and differential evolution (DE) technique for diverse conditions of the AVR in [16]. In [17], authors have developed PID-accelerated design for the AVR of the system. In [18], the authors have modified the original PSO and resulted in a simplified PSO for the AVR. The superiority of simplified PSO is shown over other optimization techniques. This paper also shows the robustness of simplified PSO for parametric uncertainties. In [19], the AVR performance was done by using the modified cost function-oriented optimization technique. The efficient AVR strategy was obtained using stochastic fractal search (SFS) to increase the accuracy and to reduce the convergence time [20]. The results verified that SFS design PID for the AVR is much better than other PID designs, i.e., many optimizing liaisons (MOL) PID. In [21], heuristic optimization built 2DOF-PI state feedback was designed for the AVR. In [22], authors have found that PIDA built on the bat algorithm is also capable to provide optimal and robust design for the AVR. In [23], the authors have done a comparative analysis of various AVR designs using recent optimization techniques, and it is seen that TLBO outperforms other optimization techniques for the AVR design. Furthermore, the performance of any algorithm depends highly on the chosen objective function. Integrated square error (ISE), integrated absolute error (IAE), and integral time-weighted-absolute error (ITAE) are some of the standard objective functions used to tune the gains of PID via optimization techniques. The objective function aims to reduce or eliminate the voltage error, and hence to achieve better AVR responses and system stability after a certain disturbance. On the other side, these optimization techniques work on a trial-and-error concept, and they are problem specific. These techniques work on the concept of finding the best solution or optimal solution considering some set of constraints or limitations. However, there are several feasible solutions to a problem, and optimization techniques will choose the best solution to the problem. However, if the operating conditions or system parameters change from the original values, then there may be a chance that obtained solution may not be the best answer to the problem. These algorithms consume a lot of time to provide the best solution, and hence the AVR needs further research and investigation, and some sought a solution which will be more feasible and accurate because of the diverse conditions of the AVR such as disturbance observer based control (DOBC) [24], hybrid extended state observer (HYESO) [25], disturbance attenuation and rejection [26], and extended observer or similar designs [27–29]. In [30, 31], authors have developed a robust active disturbance rejection controller (ADRC)/extended state observer based controller (ESOBC) for the AVR. However, the operation is limited to the disturbances and uncertainties in the generator dynamics only. In view of the abovementioned, the following are the important contributions of the present work:

(1) To study the modelling of the AVR for the power system and to develop the complete state-space model of the AVR using MATLAB 2022 software for investigation and analysis

(2) To estimate the effect of multiple irregularities due to nonlinear dynamics, parametric uncertainties, and load disturbances in each component of the AVR (i.e., amplifier, exciter, and generator)

(3) To develop the structure of multiple extended state observer-based controller (MESOBC) for the AVR of the power system and to check its design and feasibility for various considered cases of the AVR

(4) Integral square error (ISE) is used to study the performance of MESOBC for the AVR and to match its performance with recently published AVR designs for normal conditions, ±30% load voltage variation and parametric uncertainty with ±30% load voltage variation

(5) The results of MESOBC are compared with SFS-PID, MOL-PID, TLBO-PID, and TLBO-PIDA based most popular optimizing controllers by obtaining the AVR response and by calculating the peak overshoot (%), rise time, steady-state error, and ISE values

(6) Finally, the effect of disturbances including parametric uncertainties, nonlinearities, and external load disturbances that occurred in all the components are estimated and rejected from the output of the AVR. Application results are shown to guarantee the simplicity and robustness of MESOBC for the AVR over other AVR designs.

This paper is organized as follows: Section 2 introduces the preliminaries of the state-space modelling of the AVR. The detailed disturbed, uncertain, and nonlinear mathematical model for all the states is presented under the influence of external load voltage disturbance. These disturbances capture the total effect of irregularities like parametric uncertainties, nonlinearities, and external load disturbances which are commonly known as lumped disturbances. In Section 3, the multiple extended state observer (MESO) is introduced to estimate abovementioned lumped disturbances from all the states of the AVR. Then, the MESO-based controller (MESOBC) is proposed to reduce the effect of these lump disturbances from the generator output. Section 4 presents the simulation results to validate

the robustness of the proposed approach followed by concluding remarks in Section 5.

2. AVR Modeling

An AVR system comprises three primary components: amplifier, exciter, and generator, as given in Figure 1. The schematic diagram of the open loop AVR model is shown in Figure 1. The prime objective of the AVR is to regulate the synchronous generator terminal voltage (i.e., $V_g(t)$) near fixed reference voltage (i.e., $V_r(t)$) by manipulating the controller voltage (i.e., $V_c(t)$) by sensing the states like voltage across amplifier, exciter, and generator (i.e., $V_a(t)$, $V_e(t)$, and $V_g(t)$).

Based on the information of states, the controller modifies the amplifier voltage, which is fed to the exciter to manage the excitation current of the exciter. The exciter alters the rotor field current to vary the synchronous generator terminal voltage as per the diverse loading conditions. The three main components of the AVR system and their ranges are given in Table 1. The saturation, nonlinearity, and sensor dynamics are ignored during the simulation.

It is well known that the dynamics of AVR components (i.e., amplifier, exciter, and generator) with parametric uncertainties (i.e., $dK_a, dK_e, dK_g, dT_a, dT_e, dT_g$) with appropriate bounds as mentioned in Table 1 can be approximated by (1)–(3) [2–6].

$$G_a(s) = \frac{K_a + dK_a}{(T_a + dT_a)s + 1}, \tag{1}$$

$$G_e(s) = \frac{K_e + dK_e}{(T_e + dT_e)s + 1}, \tag{2}$$

$$G_g(s) = \frac{K_g + dK_g}{(T_g + dT_g)s + 1}. \tag{3}$$

Let us declare $x(t) = \begin{bmatrix} V_g(t) & V_e(t) & V_a(t) \end{bmatrix}$, $u(t) = V_c(t)$, and $y(t) = V_g(t)$ as the state, input, and output vectors, respectively. Using this declaration and (1)–(3), the state-space model of the AVR with parametric uncertainties and load disturbance can be described by (4)–(6).

$$\dot{x}_1(t) = -\left(\frac{1}{T_g}\right)x_1(t) + \left(\frac{K_g}{T_g}\right)x_2(t) + \left(\frac{-V_d - \dot{V}_d(T_g + dT_g) + dK_g x_2(t) - \dot{x}_1(t)dT_g}{T_g}\right), \tag{4}$$

$$\dot{x}_2(t) = -\left(\frac{1}{T_e}\right)x_2(t) + \left(\frac{K_e}{T_e}\right)x_3(t) + \left(\frac{dK_e x_3(t) - \dot{x}_2(t)dT_e}{T_e}\right), \tag{5}$$

$$\dot{x}_3(t) = -\left(\frac{1}{T_a}\right)x_3(t) + \left(\frac{K_a}{T_a}\right)u(t) + \left(\frac{dK_a u(t) - \dot{x}_3(t)dT_a}{T_a}\right). \tag{6}$$

Finally, these dynamics with lumped disturbances (d) are presented in the standard state-space model by (7) and (8).

$$\dot{x}(t) = \begin{bmatrix} -a_1 & b_1 & 0 \\ 0 & -a_2 & b_2 \\ 0 & 0 & -a_3 \end{bmatrix} x(t) + \begin{bmatrix} 0 \\ 0 \\ b_3 \end{bmatrix} u(t) + \begin{bmatrix} 1 & 0 & 0 \\ 0 & 1 & 0 \\ 0 & 0 & 1 \end{bmatrix} \begin{bmatrix} d_1(t) \\ d_2(t) \\ d_3(t) \end{bmatrix}, \tag{7}$$

$$y = \begin{bmatrix} 1 & 0 & 0 \end{bmatrix} x(t), \tag{8}$$

where $a_1 = (1/T_g)$, $a_2 = (1/T_e)$, $a_3 = (1/T_a), b_1 = (K_g/T_g), b_2 = (K_e/T_e), b_3 = (K_a/T_a)$ are the positive constants. The lump disturbances, d_1, d_2, and d_3 are the total effect of parametric uncertainties, external load disturbance, and nonlinearities present in generator, exciter, and amplifier systems, respectively.

$$d_1(t) = \frac{-V_d - \dot{V}_d(T_g + dT_g) + dK_g x_2(t) - \dot{x}_1(t)dT_g}{T_g}, \tag{9}$$

$$d_2(t) = \frac{dK_e x_3(t) - \dot{x}_2(t)dT_e}{T_e}, \tag{10}$$

$$d_3(t) = \frac{dK_a u(t) - \dot{x}_3(t)dT_a}{T_a}. \tag{11}$$

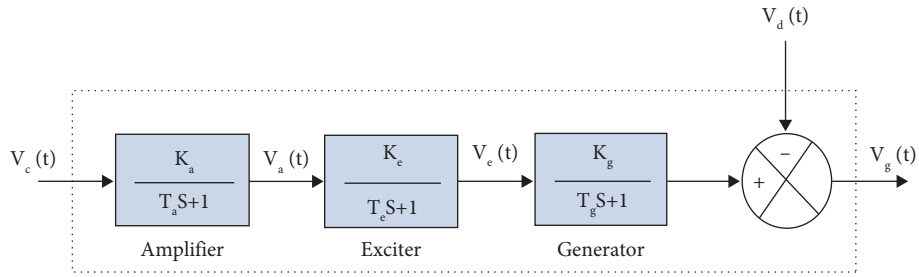

Figure 1: Open-loop schematic diagram of automatic voltage regulator (AVR) with transfer functions.

Table 1: Description of AVR components and their ranges [2, 3].

AVR components	Gain ranges	Time constant ranges
Amplifier	$10 \le K_a \le 40$	$0.02 \le T_a \le 0.1$
Exciter	$1 \le K_e \le 10$	$0.4 \le T_e \le 1$
Generator	$0.7 \le K_g \le 1$	$1 \le T_g \le 2$

The dynamics of d_1, d_2, and d_3 presented in (9)–(11) clearly indicate that the complete model of the AVR is a group of nonlinear, uncertain, and disturbed systems.

3. Multiple Extended State Observer-Based Controller (MESOBC) for AVR

The detailed model of the AVR along with the disturbances (i.e., $d_1(t), d_2(t), d_3(t)$) in each component is presented by (7)–(11). These disturbances capture the total effect of irregularities like parametric uncertainties, nonlinearities, and external load disturbances which are commonly known as lumped disturbances [24]. Based on (7), it is very well observed that $d_1(t)$ and $d_2(t)$ are mismatched types while $d_3(t)$ is matched type multichannel lumped disturbances [25]. It is proven that the estimator and controller design for tackling mismatched disturbances in real-time systems like the AVR is quite challenging [26]. In this paper, we have proposed a novel approach to estimate and control the matched as well as mismatched kinds of multiple lumped disturbances for the AVR system under Assumption 1. This approach can be further utilized for other real-time physical systems also. To reject the total effect of these multiple disturbances from the generator output, it is necessary to estimate the effect of individual disturbances first. Initially, the estimation of each lumped disturbance that exists in each component of the AVR is carried out using multiple extended state observer (MESO). In the next step, the MESO-based controller (MESOBC) is designed for compensating the total effect of lumped disturbances from the generator output as shown in Figure 2.

Assumption 1 (see [25]). The disturbance vector, $d(t)$, is composed of multiple lumped disturbances, i.e., $d_1(t), d_2(t), d_3(t)$, for the AVR are as follows:

(1) The lumped disturbance vector $d(t)$ characterizes the external disturbances, parameter uncertainties, unmodeled dynamics, and nonlinearities

(2) $d(t)$ and its derivative $\dot{d}(t)$ having bounded variation, i.e., $|d(t)| < \mu_1, |\dot{d}(t)| < \mu_2$

(3) $d(t)$ is a constant or slow time-changing lumped disturbance vector with the constant final value, i.e., $\lim_{t \longrightarrow \infty} d(t) \cong$ constant

Let us design the estimator for the generator of the AVR based on the extended state observer (ESO) [27]. The overall generator dynamics with lumped disturbance can be presented by (12).

$$\begin{aligned} \dot{x}_1(t) &= -a_1 x_1(t) + b_1 x_2(t) + d_1(t), \\ y_1(t) &= x_1(t). \end{aligned} \tag{12}$$

The exciter voltage ($x_2(t)$) is available through the appropriate sensor as input for (12). Based on the ESO methodology, the lumped disturbance $d_1(t)$ is considered as an extended state. The new state variables are formed as follows:

$$\begin{aligned} z_1(t) &= x_1(t), \\ z_2(t) &= d_1(t), \\ u_1(t) &= x_2(t), \\ y_1(t) &= z_1(t). \end{aligned} \tag{13}$$

Combining (12) and (13), the extended state model for the generator is presented by the following equations:

$$\begin{aligned} \dot{z}_1(t) &= -a_1 z_1(t) + z_2(t) + b_1 u_1(t), \\ \dot{z}_2(t) &= \dot{d}_1(t), \\ y_1(t) &= z_1(t), \end{aligned} \tag{14}$$

$$\begin{aligned} \dot{z}(t) &= \begin{bmatrix} -a_1 & 1 \\ 0 & 0 \end{bmatrix} x(t) + \begin{bmatrix} b_1 \\ 0 \end{bmatrix} u(t) + \begin{bmatrix} 0 \\ 1 \end{bmatrix} \dot{d}_1(t), \\ y_1(t) &= \begin{bmatrix} 1 & 0 \end{bmatrix} z(t). \end{aligned} \tag{15}$$

Denoting $A_1 = \begin{bmatrix} -a_1 & 1 \\ 0 & 0 \end{bmatrix}$, $B_1 = \begin{bmatrix} b_1 \\ 0 \end{bmatrix}$, $C_1 = \begin{bmatrix} 1 & 0 \end{bmatrix}$, and $h_1 = \begin{bmatrix} 0 \\ 1 \end{bmatrix}$, the ESO-1 can be designed for (15) if (A_1, C_1)

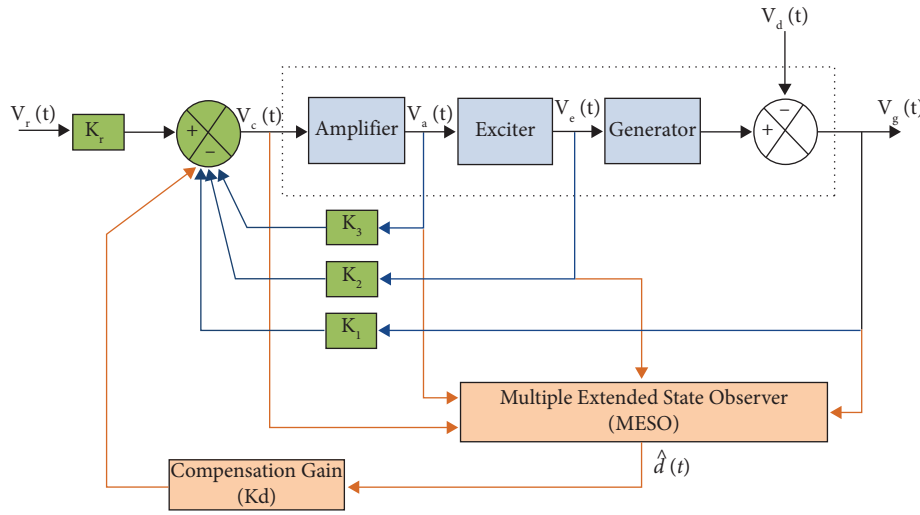

Figure 2: Schematic diagram of MESOBC for AVR.

pair is observable. The ESO-based estimated dynamics of (14) can be written as follows:

$$\begin{aligned}\dot{\hat{z}}_1(t) &= -a_1\hat{z}_1(t) + \hat{z}_2(t) + b_1u_1(t) + l_{11}\left(z_1(t) - \hat{z}_1(t)\right),\\ \dot{\hat{z}}_2(t) &= l_{12}\left(z_1(t) - \hat{z}_1(t)\right),\\ \hat{y}_1(t) &= \hat{z}_1(t),\end{aligned} \tag{16}$$

where $L_1 = \begin{bmatrix} l_{11} \\ l_{12} \end{bmatrix}$ is the ESO-1 gain vector for the generator system. Now, let us define the estimation error as $e_1(t) = z_1(t) - \hat{z}_1(t)$ and $e_2(t) = z_2(t) - \hat{z}_2(t)$. The first derivative of the estimation error vector, $e(t) = \begin{bmatrix} e_1(t) \\ e_2(t) \end{bmatrix}$, using (16) can be given by (17).

$$\dot{e}(t) = \begin{bmatrix} -a_1 - l_{11} & 1 \\ 0 & -l_{12} \end{bmatrix} e(t) + \begin{bmatrix} 0 \\ 1 \end{bmatrix} \dot{d}_1(t). \tag{17}$$

Finally, under Assumption 1, if $L_1 = \begin{bmatrix} l_{11} \\ l_{12} \end{bmatrix}$ is chosen in such a way that $\begin{bmatrix} -a_1 - l_{11} & 1 \\ 0 & -l_{12} \end{bmatrix}$ remains Hurwitz, then according to [28], the estimation error dynamics of ESO-1 in (17) converges asymptotically (i.e., $z_1(t) \cong \hat{z}_1(t)$ and $z_2(t) \cong \hat{z}_2(t)$). A similar ESO methodology can be utilized for the exciter and the amplifier dynamics to obtain the estimation of lumped disturbances, $d_2(t)$ and $d_3(t)$ with ESO-2 (i.e., $L_2 = \begin{bmatrix} l_{21} \\ l_{22} \end{bmatrix}$) and ESO-3 (i.e., $L_3 = \begin{bmatrix} l_{31} \\ l_{32} \end{bmatrix}$), respectively. The generalized ESO [29] structure of the AVR system can be presented by (18) using (7) and (8) as shown below.

$$\begin{aligned}\dot{x}(t) &= Ax(t) + Bu(t) + B_d d(t),\\ y(t) &= Cx(t),\end{aligned} \tag{18}$$

where

$$\begin{aligned}A &= \begin{bmatrix} -a_1 & b_1 & 0 \\ 0 & -a_2 & b_2 \\ 0 & 0 & -a_3 \end{bmatrix},\\ B &= \begin{bmatrix} 0 \\ 0 \\ b_3 \end{bmatrix},\\ B_d &= \begin{bmatrix} 1 & 0 & 0 \\ 0 & 1 & 0 \\ 0 & 0 & 1 \end{bmatrix},\\ C &= \begin{bmatrix} 1 & 0 & 0 \end{bmatrix}.\end{aligned} \tag{19}$$

Finally, we can design multiple ESO (i.e., ESO-1, 2, and 3)-based controller using the estimated lumped disturbances, (e.g. $\hat{d}_1(t), \hat{d}_2(t)$, and $\hat{d}_3(t)$). The control law ($u(t)$) in (19) based on the information of MESO and the state variables (x) can be given by [29]:

$$u(t) = -K_x x(t) + K_r r(t) - K_d \hat{d}(t). \tag{20}$$

By combining and rearranging (19) and (20),

$$\begin{aligned}\dot{x}(t) &= \left[A - BK_x\right]x(t) + K_r r(t) - K_d\hat{d}(t) + B_d d(t),\\ y(t) &= Cx(t),\end{aligned} \tag{21}$$

where K_x, K_r, and K_d are the state feedback, reference input, and compensation gain vectors, respectively. K_x is designed initially using any suitable state-feedback method to ensure that the matrix $(A - BK_x)$ remains Hurwitz. The other gain vectors are designed with (A, B) pair controllable and (A, C) pair observable for asymptotic stability of (21) as follows [25, 29]:

$$\begin{aligned}K_r &= -\left[C\left(A - BK_x\right)^{-1}B\right]^{-1},\\ K_d &= -\left[C\left(A - BK_x\right)^{-1}B\right]^{-1} \times C\left(A - BK_x\right)^{-1}B_d.\end{aligned} \tag{22}$$

4. Results and Analysis of MESOBC for AVR

This paper presents an initial approach for designing the MESOBC for the AVR of the power system. At first, the critical literature review of the problem is presented with the formulation of the research gaps for the AVR problem. The mathematical model of the AVR is presented in Section 2 with complete mathematical modelling of MESOBC for the AVR in Section 3. After designing the MESOBC for the AVR, the next step is to move to the next step of investigations and to carry out exhaustive investigations for the AVR of the power system using MESOBC. The integral squared error (ISE) is chosen as the objective function to minimize the voltage error as well as to match the output of MESOBC analytically and graphically. MESOBC performance is matched with recent and powerful controller designs such as SFS-PID [20], MOL-PID [20], teaching-learning optimization algorithm-PID [23], and teaching-learning optimization algorithm-PID with accelerator (PIDA) [23] for various considered cases. Based on Table 1, the simulation parameters with appropriate units for the AVR are $K_a = 10, K_e = 1, K_g = 1, T_a = 0.1, T_e = 0.4, T_g = 1$. The state-space matrices for the AVR using the simulation parameters are given by the following equation:

$$A = \begin{bmatrix} -1 & 1 & 0 \\ 0 & -2.5 & 2.5 \\ 0 & 0 & -10 \end{bmatrix},$$
$$B = \begin{bmatrix} 0 \\ 0 \\ 100 \end{bmatrix},$$
$$B_d = \begin{bmatrix} 1 & 0 & 0 \\ 0 & 1 & 0 \\ 0 & 0 & 1 \end{bmatrix}, \quad (23)$$
$$C = \begin{bmatrix} 1 & 0 & 0 \end{bmatrix}.$$

Using the standard test for (23), it is clear that (A, B) pair is controllable and (A, C) pair is observable. Hence, the design of the controller and observer is further investigated. In this paper, the multiple ESO (MESO)-based controller methodologies have been introduced for all three channels (i.e., amplifier, exciter, and generator) of the AVR to achieve the robust performance against lumped disturbances like parametric uncertainties, nonlinearities, and external load disturbances. As discussed in Section-3, the ESO-1, 2, and 3 are designed for generator, exciter, and amplifier, respectively. The MESO gain vectors are chosen using (17) for the convergences of ESOs are $L_1 = \begin{bmatrix} 1.6 \\ -1.7 \end{bmatrix}, L_2 = \begin{bmatrix} 1.5 \\ 4 \end{bmatrix}, L_3 = \begin{bmatrix} -6 \\ 4 \end{bmatrix}$. Finally, the MESO-based controller (MESOBC) is implemented for compensating the total effects of lumped disturbances from the output (i.e., generator) of the AVR using (20)–(22). Accordingly, the state-feedback (K_x), reference input (K_r), and disturbance compensation (K_d) gain vectors are obtained as $K_x = [85.9560\ 9.18\ 0.765], K_r = 96$, and $K_d = [10.044\ -0.3460\ -0.01]$.

At first, the output of MESOBC is evaluated for normal conditions of AVR. The terminal voltage in p.u. is shown in Figure 3 and matched with SFS-PID, MOL-PID, TLBO-PID, and TLBO-PIDA under similar normal conditions. It is seen that terminal voltage deviates and unable to settle quickly to the reference value through SFS-PID, MOL-PID, and TLBO-PID. However, the output of TLBO-PIDA is much faster than TLBO-PID in reaching back to 1 p.u. On the other side, MESOBC is quick enough to take the terminal voltage to 1.0 p.u. without any oscillations within a few seconds only. The analytical performance is given in Table 2 for these control actions for AVR, and it is seen that the peak overshoot (%) obtained via MESOBC reduces to 2.3177% in comparison to 23.0428% by TLBO-PID, 23.4% by SFS-PID, 14.88% by MOL-PID, and 1.0029% by TLBO-PIDA. The rise time of MESOBC is 0.16 seconds, whereas the rise time of TLBO-PID is 0.142 seconds, 0.46 for TLBO-PIDA, 0.35 for SFS-PID, and 0.432 by MOL-PID. The obtained value of ISE via MESOBC is 0.05155, and it is much lesser when matched with SFS-PID, MOL-PID, TLBO-PID, and TLBO-PIDA. It is also seen that the steady state (ss) error is zero for all three controllers.

In the second step, the ±30% load voltage is varied, and Figure 4 shows the actual and estimated load voltage variation through MESOBC. The performance of MESOBC is evaluated for load voltage variation as given in Figure 4 and matched with TLBO-PID and TLBO-PIDA. The percentage peak overshoot reduces to 30.0033% through MESOBC in comparison to the percentage peak overshoot of 30.1211% by TLBO-PID and 30.0180% by TLBO-PIDA. The SS error is minimum for MESOBC for ±30% load voltage variations. The obtained ISE value is also minimum when matched with other controllers for the AVR. The complete analytical result for this case is given in Table 3. The graphical results are shown in Figure 5, and it is clearly seen that MESOBC is much faster and more accurate in reaching the SS error to zero after the voltage varied at different instants of the time. However, the results of TLBO-PID and TLBO-PIDA are struggling to take the terminal voltage to zero after each disturbance.

In the next step, +50% parametric uncertainties are applied to T_g and K_g, and ±30% load voltage varied and the performance of MESOBC is evaluated for the AVR of the system. The numerical results are given in Table 4, and it is seen that the ISE value of TLBO-PID is 0.1188 and the ISE value obtained via TLBO-PIDA is 0.2395. However, the ISE value of MESOBC is 0.1 and much lesser when matched with TLBO-PID and TLBO-PIDA. The peak overshoot (%) and steady-state error are also minimum for MESOBC for the AVR when parametric uncertainties as well as load voltage are simultaneously varied at various time instants. The graphical results of Figure 6 verify that MESOBC is a much better control action for the AVR for this case also. Figure 7 shows the estimation of generator total disturbance under +50% parametric uncertainties (T_g and K_g) and ±30% load voltage variation. It is observed that MESOBC is capable enough to estimate the generator total disturbance for this

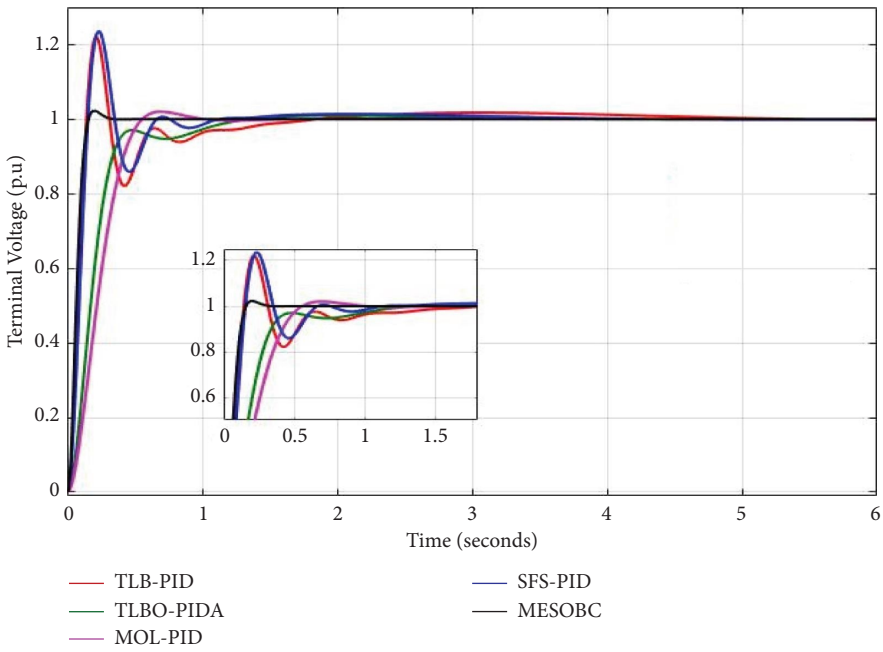

Figure 3: Response of terminal voltage under normal conditions.

case also and quick enough to respond to ±30% load voltage variations. Now the −50% parametric uncertainties are applied in (T_g and K_g) and ±30% load voltage variation for the AVR of the system. The calculated various values are given in Table 5. Here also, the MESOBC outperforms TLBO-PID and TLBO-PIDA in view of peak overshoot (%), SS error, and ISE value. Figure 8 shows the terminal voltage response with estimated generate disturbance as given in Figure 9 through MESOBC. The results show that MESOBC is showing promising results for this case also when matched with TLBO-PID and TLBO-PIDA.

4.1. Sensitivity Analysis. At last, the robustness of MESOBC-based AVR is also carried out by changing the amplifier parameters, i.e., K_a (amplifier gain) and T_a (time constant of the amplifier) ±50% from the original values. The results are given in Table 6. The SS error is zero for all positive and negative variations from the original amplifier parameters. The ISE values are comparable and a very small change was observed for positive and negative variations from the original values. There is not much change observed in the peak overshoot (%). The reason is due to matched uncertainty of the amplifier via MESOBC as the output of the controller is fed as controlled input to the amplifier in the AVR system. Figures 10 and 11 show the results of terminal voltage for the AVR using MESOBC for +50% uncertainties in T_a and K_a. The results show that MESOBC obtained terminal voltage is oscillation free and reaches 1.0 p.u. much faster when matched with TLBO-PID and TLBO-PIDA. Figures 12 and 13 show the AVR results for positive, negative, and original parameters, and it is seen that parametric uncertainties hardly affect the results of the MESOBC-based AVR. The robustness is also performed by varying the ±50% uncertainties in exciter parameters such as K_e (exciter gain) and T_e (tie constant of the exciter). The various calculated values are given in Table 7. The peak overshoot (%) is higher for +50% variations in T_e which is 9.2195 and −50%; variation in K_e also results in a higher peak overshoot of 11.6754. The reason is mismatched uncertainty as the exciter is next to the amplifier and amplifier output work as input to the exciter. However, this much change is very rare in the power system. Figures 14 and 15 show the comparative results of the AVR using MESOBC for positive, negative, and original values, and hence can be said that MESOBC is robust for these wider variations from the original value. At last, the robustness is also obtained via varying the generator gain and time constant over the wider range. The system response specifications are given in Table 8 for a wider change from the original values. Table 8 shows that varying generator parameters increase the overshoot in MESOBC-based AVR responses. However, SS error and ISE values are comparable. Figures 16 and 17 show the result of MESOBC-based AVR

Table 2: Dynamic response specification of AVR with normal condition.

Method	Peak overshoot (%)	Rise time (seconds)	Steady-state error	ISE
SFS-PID [20]	23.4	0.35	0	0.075
TLBO-PID [23]	23.0428	0.142	0	0.07248
MOL-PID [20]	14.88	0.432	0	0.1626
TLBO-PIDA [23]	1.0029	0.46	0	0.1304
MESOBC (presented)	2.3177	0.16	0	0.05155

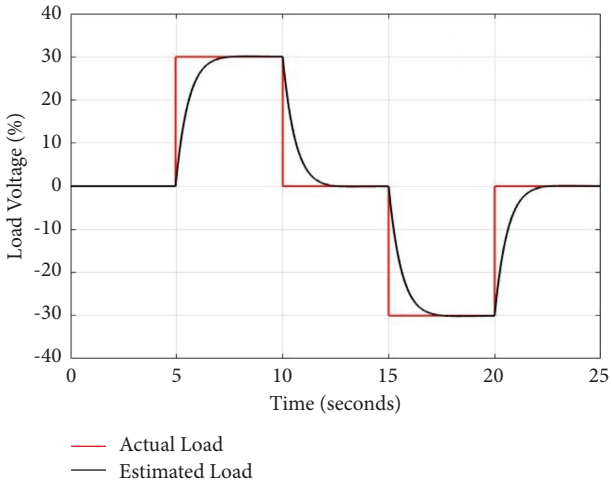

Figure 4: Estimation of ±30% load voltage variation using MESOBC.

Table 3: Dynamic response specification of AVR under ±30% load voltage variation.

Method	Peak overshoot (%)	Steady-state error	ISE
TLBO-PID [23]	30.1211	−0.0008324	0.1018
TLBO-PIDA [23]	30.0180	0.00018	0.181
MESOBC (presented)	30.0033	−0.000034	0.075

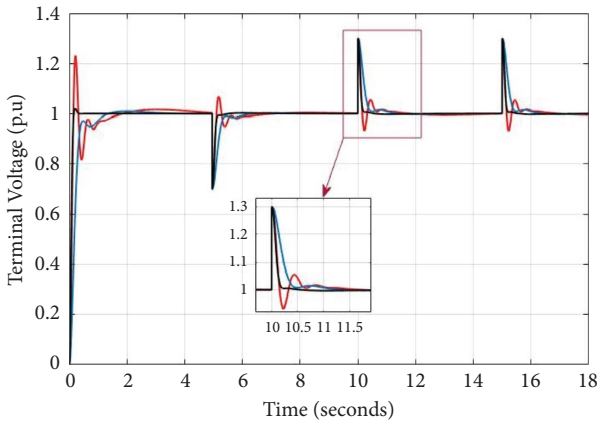

Figure 5: Response of terminal voltage under variation of ±30% load voltage.

for uncertainty in generator parameters. The graphical results of Figures 16 and 17 verify the numerical results of Table 8 except higher overshoot seen in the AVR responses. However, this much amount of change in amplifier, exciter, and generator parameters of the AVR system is rare in a realistic environment, and hence it can be said that the

Table 4: Dynamic response specification of AVR under +50% parametric uncertainties in T_g and ±30% load voltage variation.

Method	Peak overshoot (%)	Steady-state error	ISE
TLBO-PID [23]	30.1180	−0.0002873	0.1188
TLBO-PIDA [23]	30.0279	0.0002792	0.2395
MESOBC (presented)	30.0194	0.0002054	0.1

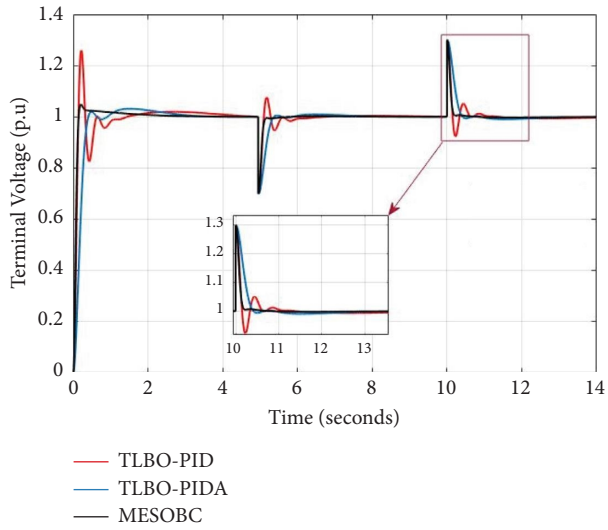

Figure 6: Response of terminal voltage under +50% parametric uncertainties (T_g and K_g) and ±30% load voltage variation.

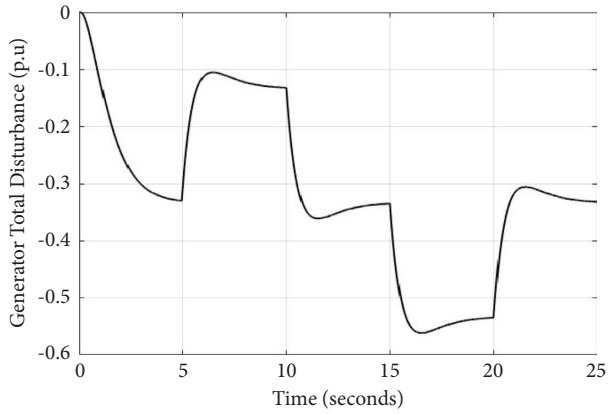

Figure 7: Estimation of generator total disturbance under +50% parametric uncertainties in (T_g and K_g) and ±30% load voltage variation.

Table 5: Dynamic response specification of AVR under −50% parametric uncertainties in T_g and ±30% load voltage variation.

Method	Peak overshoot (%)	Steady-state error	ISE
TLBO-PID [23]	30.3271	−0.003131	0.1498
TLBO-PIDA [23]	30.0200	0.0002002	0.3224
MESOBC (presented)	30.0081	−0.00008262	0.133

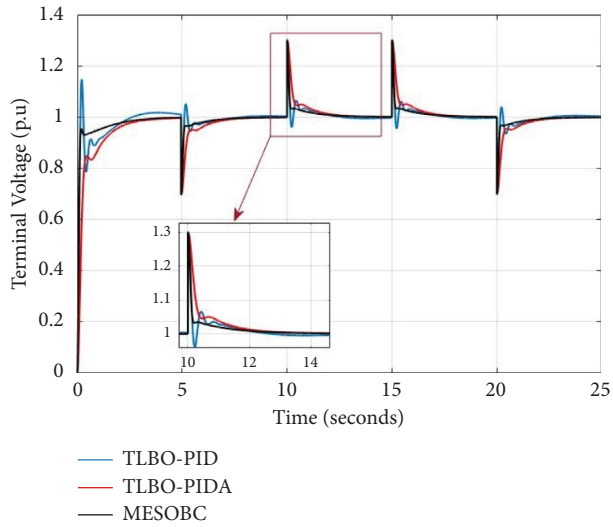

Figure 8: Response of terminal voltage under −50% parametric uncertainties in (T_g and K_g) and ±30% load voltage variation.

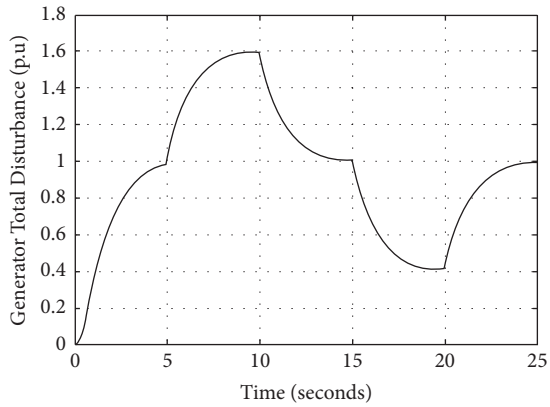

Figure 9: Estimation of generator total disturbance under −50% parametric uncertainties in (T_g and K_g) and ±30% load voltage variation.

Table 6: Robust response specification of MESOBC-based AVR under ±50% uncertainties in amplifier.

Parameter	Uncertainty (%)	Peak overshoot (%)	Steady-state error	ISE
T_a	+50	2.6715	0	0.0529
	−50	2.3120	0	0.05031
K_a	+50	2.0110	0	0.05026
	−50	4.9922	0	0.05566

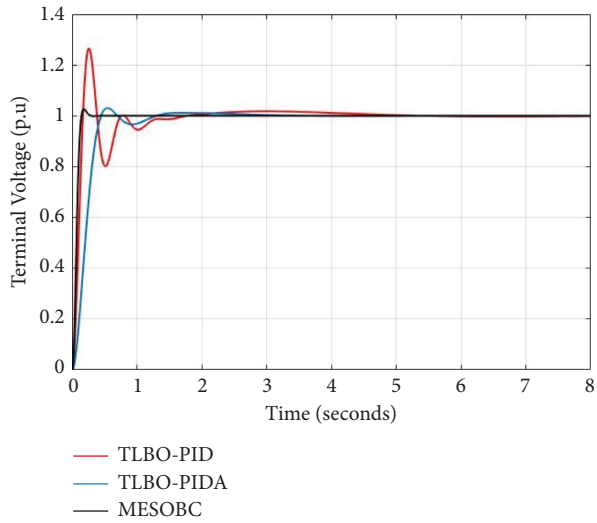

FIGURE 10: Response of terminal voltage with +50% uncertainties in T_a.

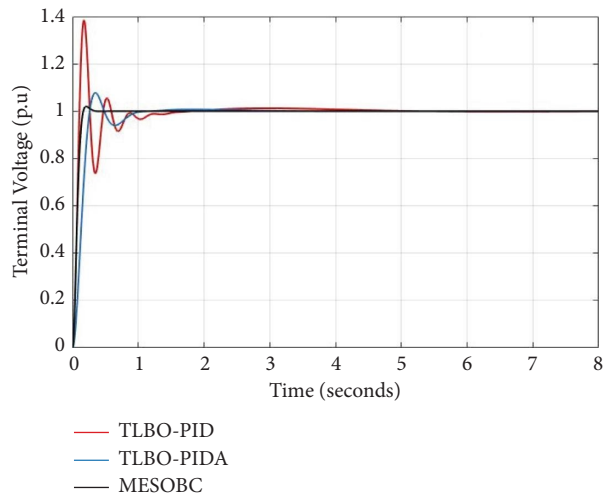

FIGURE 11: Response of terminal voltage with +50% uncertainties in K_a.

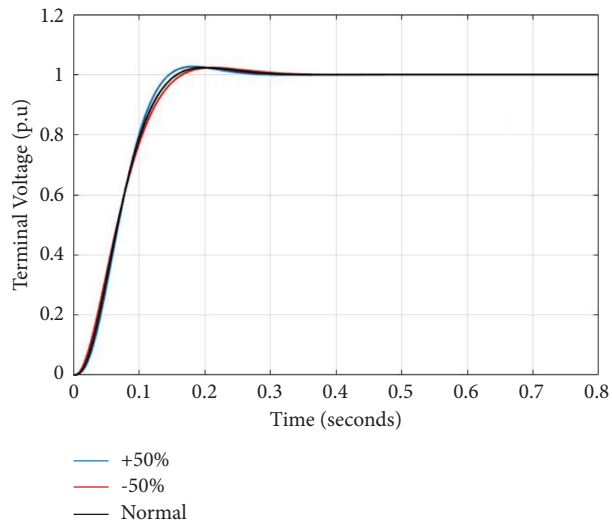

FIGURE 12: Response of terminal voltage using MESOBC for normal and ±50% uncertainties in T_a.

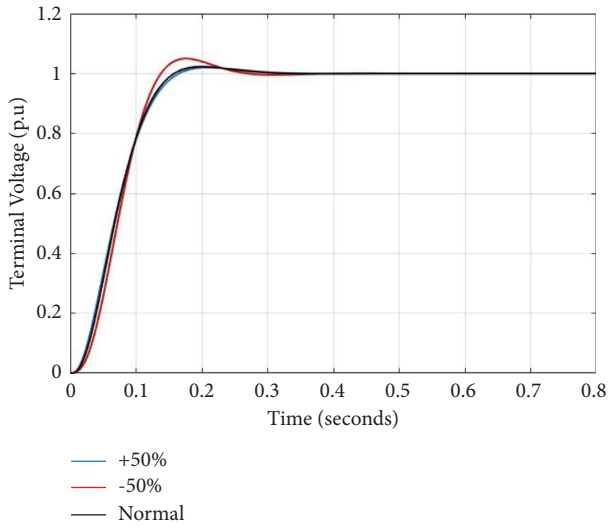

Figure 13: Response of terminal voltage using MESOBC for normal and ±50% uncertainties in K_a.

Table 7: Robust response specification of MESOBC-based AVR under ±50% uncertainties in exciter.

Parameter	Uncertainty (%)	Peak overshoot (%)	Steady-state error	ISE
T_e	+50	9.2195	0	0.05975
	−50	0	0	0.04319
K_e	+50	0	0	0.04538
	−50	11.6754	0	0.06811

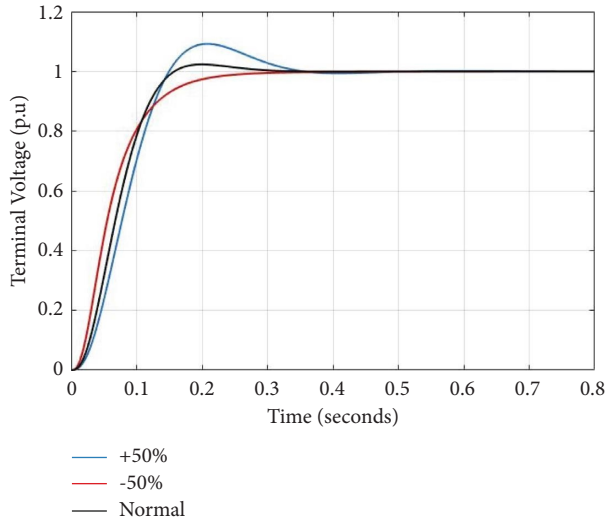

Figure 14: Response of terminal voltage using MESOBC for normal and ±50% uncertainties in T_e.

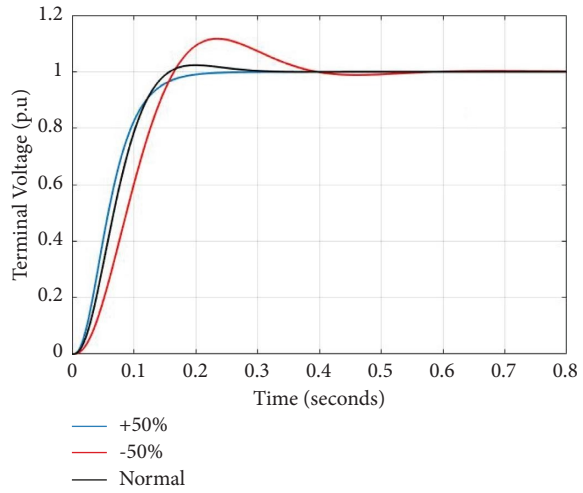

Figure 15: Response of terminal voltage using MESOBC for normal and ±50% uncertainties in K_e.

Table 8: Robust response specification of MESOBC-based AVR under ±50% uncertainties in generator.

Parameter	Uncertainty (%)	Peak overshoot (%)	Steady-state error	ISE
T_g	+50	1.8350	0	0.06953
	−50	26.6504	0	0.03877
K_g	+50	17.1327	0	0.04196
	−50	0	0	0.09239

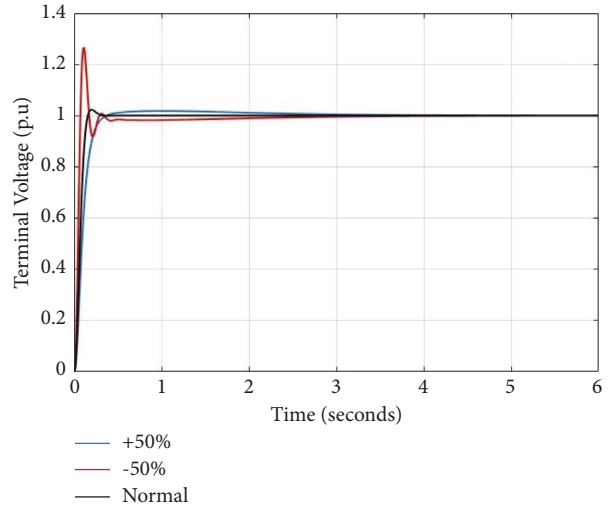

Figure 16: Response of terminal voltage using MESOBC for normal and ±50% uncertainties in T_g.

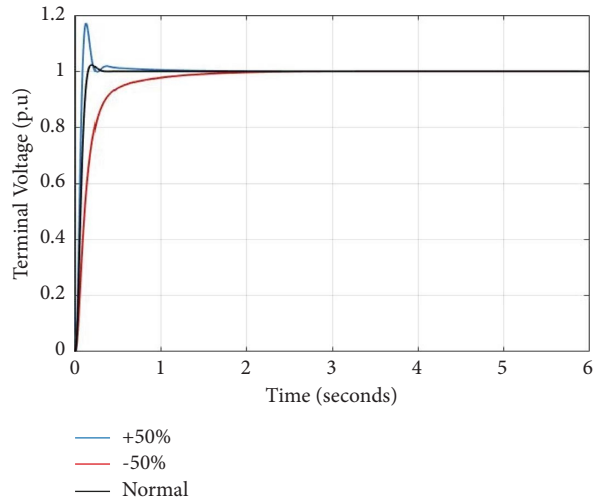

Figure 17: Response of terminal voltage using MESOBC for normal and ±50% uncertainties in K_g.

proposed MESOBC-based AVR is robust and much more suitable for wider operating conditions.

5. Conclusions

The main objective of the proposed work is to design and perform the robustness analysis of MESOBC for the uncertain and nonlinear AVR model of the power system. The MESOBC has the capability to regulate the current status of each state of the AVR system. This is achieved by estimating and rejecting the individual effect of nonlinearities, parametric uncertainties, and load disturbances in all three components of the AVR. Following conclusions are drawn from the present study:

(i) The performance of MESOBC is matched with published AVR designs by calculating peak overshoot, rise time, and steady-state error for the AVR

(ii) The ISE value is calculated to match the output of MESOBC, TLBO-PID and TLBO-PIDA, and SFS-PID and MOL-PID for investigated cases. It is observed by the graphical and analytical results that the MESOBC outperforms other AVR designs by reducing the ISE value to the best possible value for normal conditions, ±30% load voltage variation, +50% parametric uncertainties, and ±30% load voltage variation and for −50% parametric uncertainties and ±30% load voltage variation. The graphical AVR results support analytical results.

(iii) The robustness analysis of MESOBC is carried out through the sensitivity analysis in view of ±50% uncertainties in amplifier and ±50% uncertainties in exciter for the AVR of the power system, and it is seen that MESOBC has better capability to estimate each state of the power system and shows robust performance under diverse parametric uncertainties and load disturbances. It is also seen that overshoot increases slightly by altering the amplifier and exciter parameters (±50% from nominal value); however, this amount of change is rare in the power system and hence acceptable for the AVR.

(iv) Furthermore, the present research work can be extended via designing the PSS and by finding the optimal values of PSS using new and advance optimization algorithms. The PSS can be coordinated with MESOBC for the AVR.

(v) The present research work has enough scope for the real time design and analysis using Opal-RT or real time digital simulation (RTDS) platforms

Data Availability

No data were used to support this study.

Conflicts of Interest

The authors declare that they have no conflicts of interest.

References

[1] A. Ula and A. R. Hasan, "Design and implementation of a personal computer based automatic voltage regulator for a synchronous generator," *IEEE Transactions on Energy Conversion*, vol. 7, no. 1, pp. 125–131, 1992.

[2] A. H. Kiam, G. Chong, and L. Yun, "PID control system analysis, design, and technology," *IEEE Transactions on Control Systems Technology*, vol. 13, no. 4, pp. 559–576, 2005.

[3] J. A. Seul and R. C. Dorf, "Analytic PIDA controller design technique for a third order system," in *Proceedings of the 35th IEEE Conference on Decision and Control*, vol. 3, pp. 2513–2518, Kobe, Japan, December 1996.

[4] G. Mallesham and A. Rajani, "Automatic tuning of PID controller using fuzzy logic," in *Proceedings of the 8th International Conference on Development and Application Systems*, Suceava, Romania, May 2006.

[5] I. Petras, "The fractional—order controllers: methods for their synthesis and application," 2000, https://arxiv.org/abs/math/0004064.

[6] V. Kumar and A. P. Mittal, "Parallel fuzzy P+fuzzy I+fuzzy D controller: design and performance evaluation," *International Journal of Automation and Computing*, vol. 7, no. 4, pp. 463–471, 2010.

[7] D. E. Goldberg, *Genetic Algorithms in Search Optimization and Machine Learning*, Addison Wesley Publishers, Edmonton, AB, Canada, 1989.

[8] D. K. Sambariya, R. Gupta, and R. Prasad, "Design of optimal input-output scaling factors based fuzzy PSS using bat algorithm," *Engineering Science and Technology, an International Journal*, vol. 19, no. 2, pp. 991–1002, 2016.

[9] E. Rashedi, H. Nezamabadi-Pour, and S. Saryazdi, "GSA: a gravitational search algorithm," *Information Sciences*, vol. 179, no. 13, pp. 2232–2248, 2009.

[10] Z. W. Geem, J. H. Kim, and G. V. Loganathan, "A new heuristic optimization algorithm: harmony search," *Simulation*, vol. 76, no. 2, pp. 60–68, 2001.

[11] P. Yadav, R. Kumar, S. Panda, and C. Chang, "An intelligent tuned harmony search algorithm for optimisation," *Information Sciences*, vol. 196, pp. 47–72, 2012.

[12] R. V. Rao, V. J. Savsani, and D. P. Vakharia, "Teaching–Learning-Based Optimization: an optimization method for continuous non-linear large scale problems," *Information Sciences*, vol. 183, no. 1, pp. 1–15, 2012.

[13] R. V. Rao, V. J. Savsani, and D. P. Vakharia, "Teaching learning based optimization: a novel method for constrained mechanical design optimization problems," *Computer-Aided Design*, vol. 43, no. 3, pp. 303–315, 2011.

[14] Z. L. Gaing, "A particle swarm optimization approach for optimum design of PID controller in AVR system," *IEEE Transactions on Energy Conversion*, vol. 19, no. 2, pp. 384–391, 2004.

[15] A. Soundarrajan, S. Sumathi, and C. Sundar, "Ant colony optimization based PID tuning for AVR in autonomous power generating systems," *International Journal on Recent Trends in Engineering & Technology*, vol. 3, no. 4, pp. 125–129, 2010.

[16] H. Gozde and M. C. Taplamacioglu, "Comparative performance analysis of artificial bee colony algorithm for automatic voltage regulator (AVR) system," *Journal of the Franklin Institute*, vol. 348, no. 8, pp. 1927–1946, 2011.

[17] D. Puangdownreong, "Application of current search to optimum PIDA controller design," *Intelligent Control and Automation*, vol. 03, no. 4, pp. 303–312, 2012.

[18] S. Panda, B. K. Sahu, and P. K. Mohanty, "Design and performance analysis of PID controller for an automatic voltage regulator system using simplified particle swarm optimization," *Journal of the Franklin Institute*, vol. 349, no. 8, pp. 2609–2625, 2012.

[19] E. Celik and R. Durgut, "Performance enhancement of automatic voltage regulator by modified cost function and symbiotic organisms search algorithm," *Engineering Science and Technology, an International Journal*, vol. 21, no. 5, pp. 1104–1111, 2018.

[20] E. Celik, "Incorporation of stochastic fractal search algorithm into efficient design of PID controller for an automatic voltage regulator system," *Neural Computing & Applications*, vol. 30, no. 6, pp. 1991–2002, 2018.

[21] I. Eke, M. Saka, H. Gozde, Y. Arya, and M. C. Taplamacioglu, "Heuristic optimization based dynamic weighted state feedback approach for 2DOF PI-controller in automatic voltage regulator," *Engineering Science and Technology, an International Journal*, vol. 24, no. 4, pp. 899–910, 2021.

[22] D. K. Sambariya and D. Paliwal, "Design of PIDA controller using BAT algorithm for AVR power system," *Advances in Energy and Power*, vol. 4, no. 1, pp. 1–6, 2016.

[23] A. M. Mosaad, M. A. Attia, and A. Y. Abdelaziz, "Comparative performance analysis of AVR controllers using modern optimization techniques," *Electric Power Components and Systems*, vol. 46, no. 19-20, pp. 2117–2130, 2018.

[24] W. H. Chen, J. Yang, L. Guo, and S. Li, "Disturbance-observer-based control and related methods—an overview," *IEEE Transactions on Industrial Electronics*, vol. 63, no. 2, pp. 1083–1095, 2016.

[25] R. V. Gandhi and D. M. Adhyaru, "Hybrid extended state observer based control for systems with matched and mismatched disturbances," *ISA Transaction*, vol. 106, pp. 61–73, 2020.

[26] L. Guo and W.-H. Chen, "Disturbance attenuation and rejection for systems with nonlinearity via DOBC approach," *International Journal of Robust and Nonlinear Control*, vol. 15, no. 3, pp. 109–125, 2005.

[27] J. Han, "Extended state observer for a class of uncertain plants," *Control and Decision*, vol. 10, no. 1, pp. 85–88, 1995.

[28] B. Z. Guo and Z. L. Zhao, "On the convergence of an extended state observer for nonlinear systems with uncertainty," *Systems and Control Letters*, vol. 60, no. 6, pp. 420–430, 2011.

[29] S. Pawar, R. H. Chile, and B. M. Patre, "Design of Generalized Extended State Observer Based Control for Nonlinear Systems with Matched and Mismatched Uncertainties," in *Proceedings of the 2017 Indian Control Conference (ICC)*, pp. 65–71, Indian Institute of Technology, Guwahati, India, January 2017.

[30] A. Mandali, L. Dong, and A. Morinec, "Robust Controller Design for Automatic Voltage Regulation," in *Proceedings of the 2020 American Control Conference*, Denver, CO, USA, July 2020.

[31] R. Angu and R. K. Mehta, "Effect of extended state observer and automatic voltage regulator on synchronous machine connected to infinite bus power system," *Journal of the Institution of Engineers: Serie Bibliographique*, vol. 99, no. 2, pp. 147–156, 2018.